

# INTERNATIONAL SCIENTIFIC CONFERENCE

20-22 November 2025, GABROVO



# FINITE ELEMENT ANALYSIS OF A RADIAL SHAFT SEAL WITH A NOVEL MESH REFINEMENT APROACH

### Georgi Panchev

Trelleborg Sealing Solutions Bulgaria LTD, Christofor Columb 80, Sofia, Bulgaria \*Corresponding author: georgi.panchev@trelleborg.com

#### Abstract

This study presents a holistic analysis of radial shaft seals by means of 3D finite element analysis (FEA). Special emphasis is given to the sealing edge, examining its complex behavior under operating conditions, and including the surface roughness profile on the microscale for detailed 3D model simulation. In addition, the underlying equations of hyperelastic material models, which are important for appropriately simulating the elastomeric parts of the seal, are discussed to give a sound mathematical foundation to the simulations. This encompasses thorough discussions on boundary conditions and mathematical models necessary for replicating the complicated deformation and contact mechanics of the sealing interface. The tangential distortion of the sealing edge, an important factor determining sealing performance, is examined using multiscale models linking macroscopic seal geometry to microscopic surface roughness.

Keywords: radial shaft seal, FEA, distortion.

#### INTRODUCTION

Radial shaft seals, also referred to as radial lip seals, are basic elements widely used in a variety of mechanical and automotive engineering applications. Their main purpose is to create a strong barrier, withstanding fluid exchange at shaft passages and sealing effectively against fluid leakage, while also keeping out external contaminants like dirt and dust from important mechanical components. These seals have various benefits, such as their inexpensiveness, low space demands, simplicity of installation and ability to seal a wide range of applications with different operating conditions.

Typically, a radial lip seal consists of an elastomeric body, usually made from materials such as nitrile butadiene rubber, polyurethane or fluoroelastomer, bonded to a metallic case – *Fig.1*. The construction has one or more elastomeric lips, commonly garter spring-supported, that press radially against

the rotating shaft. The synergy of lip deformation and spring extension provides constant contact with the shaft, ensuring an effective seal. In the static situation, the interference between the sealing ring's inner diameter and the shaft and the spring load push the sealing edge against the shaft, guaranteeing static tightness. Under dynamic operation conditions, the relative motion of the rotating shaft causes a thin hydrodynamic lubricating film to form between the seal lip and the shaft surface, which is vital for minimizing frictional forces and limiting the contact temperatures. The lubricating film facilitates the reverse pumping effect, whereby fluid entering the sealing gap is pumped back from the air side to the fluid side with the result that the seal is in a dynamic leak-tight state. The asymmetrical configuration of the sealing element has the effect of further promoting this reverse pumping effect. The contact stress distribution also has asymmetric shape which can be

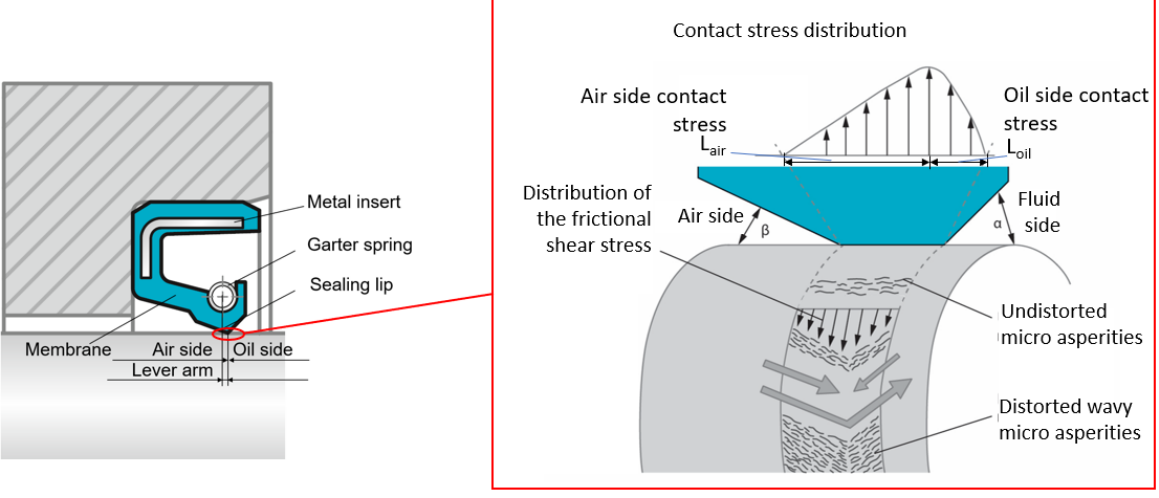


Fig. 1. (A) Components of the radial shaft seal (B) Sealing edge distortion.

described with the distance  $L_{air}$  (from the beginning of the contact on the air side to the maximal stress value) and  $L_{oil}$  (from maximal stress value until end of the contact from oil side). Typically  $L_{air} > L_{oil}$  the ratio is defined  $S = L_{oil} / L_{air}$  such that S < 1 correspond to back pumping sealing edge.

In spite of several decades of developments giving rise to significant empirical improvements and sophisticated designs, problems still persist, particularly in applications involving high pressures, which can greatly increase the mechanical and thermal stresses on the sealing lip. The trade-off between leak-free performance and the need for a long service life remains a critical factor since a slight amount of leakage can, on occasions, improve lubrication and increase the operating life of the seal.

The complex interaction between these scales is essential for describing the tribological performance and sealing mechanisms of radial shaft seals, with regard to the micromechanical contact deformations experienced during shaft rotation [1]. A multiscale strategy is necessary to accurately describe the large macroscopic deformations due to the hyperelastic material behavior of elastomers, in conjunction with microscopic tangential distortions of the sealing edge surface within the contact area [2]. This encompasses the combination of numerical studies with experimental observations, such as

those using a hollow glass shaft for in situ visual contact analyses, to verify the complex phenomena experienced at the sealing interface. From this basis, the application of finite element analysis becomes essential for calculating both the macroscopic deformation of the seal and the microscopic distortion of the sealing edge surface roughness. Numerical analyses, in contrast to experimental test rigs, are not subject to external disturbances, enabling focused studies of various influences on the sealing mechanism. This permits exact investigations into parameters such as contact pressure distribution and tangential displacement on a microscale, critical for predicting seal performance and lifetime. The strong computational power of FEA allows for a close examination of elastohydrodynamic and thermos-elastohydrodynamic behaviors, progressing from classical axisymmetric assumptions to include three-dimensional nonaxisymmetric effects that play an important role in lip deformation and sealing integrity [3]. This in-depth analysis is continued in understanding the impact of wear on the performance of radial lip seals, using numerical simulations to compare different sealing edge wear states [4]. This is especially applicable considering that the surface roughness exposed to the lubricant and shaft in a lip seal is in a highly compressed state, requiring models capable of deforming surface

roughness according to real radial lip seal data [5].

The transfer of measured wear states from experimental investigations to 3D multiscale models enables the simulation of both macroscopic deformation of the whole radial lip seal and microscopic deformations within the contact area between the sealing edge and the shaft surface. Thus, numerical methodologies, e.g. mixed elastohydrodynamic lubrication models, are commonly utilized to investigate the complicated sealing behavior by coupling hydrodynamic lubrication, asperity contact and deformation analyses through iterative computational steps [6]. This enables gaining a holistic understanding of the complicated interaction between fluid mechanics and solid mechanics, resulting in more precise predictions of seal performance and lifetime [7].

The current study presents a new interpretation of the 3D finite element simulation approach by Grün et al [3]. The numerical implementation includes a self-developed approach for the finite-element discretization of the seal. A new refinement approach is presented for the 3D mesh of the sealing edge as well. The FEA results for the sealing edge distortion and contact stress are interpreted in terms of the newly introduced S value characterizing the pumping performance of the seal.

#### **EXPOSITION**

This section outlines the methodologies used for 3D finite element analyses of radial shaft seals, highlighting the computational methods and material models used. A main emphasis is placed on the hyperelastic constitutive models required to realistically describe the elastomeric components, with a clear explanation of the meshing techniques, especially for the all-important sealing edge. The methodology also includes the use of special contact algorithms and the application of boundary conditions needed to model the realistic operating environment of the seal. For example, an axisymmetric 2D

model may be created within commercial FEA packages, assuming isotropic and homogeneous material properties for components such as the steel frame and shaft (linearly elastic) and the elastomeric ring (represented as a Mooney-Rivlin material). On the other hand, 3D models are used to capture non-axisymmetric effects, e.g., those caused by shaft eccentricity or dynamic operating conditions, which have a major impact on contact pressure distribution and sealing performance. These 3D models can include advanced modeling techniques required to realistically capture complicated deformation patterns and assess the effects of such distortions on the behavior of the seal under different operating conditions as described by the Kammüller functioning hypothesis [8]. In particular, the FEA approach enables including Kammüller distortion hypothesis and the creation of rough sealing edge surfaces, facilitating the investigation of microscopic effects in the sealing contact by mapping measured wear states into the 3D multiscale model. In addition, the use of hyperelastic material models, e.g., the Mooney-Rivlin or Ogden models, is essential to accurately capture the large strain behavior of the elastomeric seal material under operational loads, which differs considerably from linear elastic behavior. These models, widely available in commercial FEA software packages such as Abaqus and ANSYS, are vital to precisely predict the material response of the elastomer under different loading scenarios, maintaining the fidelity of the simulation results.

#### Mathematical models for FEA

The description and solution of large hyperelastic deformations in radial shaft seals requires a fundamental understanding of elasticity theory, hyperelastic material models and mathematical formulation and discretization.

The stress state of an element can be described by the stress tensor [9].



$$\sigma = \begin{bmatrix} \sigma_{xx} & \tau_{xy} & \tau_{xz} \\ \tau_{yx} & \sigma_{yy} & \tau_{yz} \\ \tau_{zx} & \tau_{zy} & \sigma_{zz} \end{bmatrix}$$
(1)

Here, normal stresses  $\sigma_{ij}$  and shear stresses  $\tau_{ij}$  are differentiated from each other. Stresses on a body lead to deformations. In this case, strains  $\varepsilon_{ij}$  and slip  $\gamma_{ij}$  can be distinguished. Analogous to the stress tensor, the strain tensor for infinitesimal displacements  $u_x$ ,  $u_y$  and  $u_z$  is thus

$$\varepsilon = \begin{bmatrix} \varepsilon_{xx} & \varepsilon_{xy} & \varepsilon_{xz} \\ \varepsilon_{yx} & \varepsilon_{yy} & \varepsilon_{yz} \\ \varepsilon_{zx} & \varepsilon_{zx} & \varepsilon_{zz} \end{bmatrix} = \begin{bmatrix} \varepsilon_{xx} & \frac{1}{2}\gamma_{xy} & \frac{1}{2}\gamma_{xz} \\ \frac{1}{2}\gamma_{yx} & \varepsilon_{yy} & \frac{1}{2}\gamma_{yz} \\ \frac{1}{2}\gamma_{zx} & \frac{1}{2}\gamma_{zy} & \varepsilon_{zz} \end{bmatrix}$$
(2)

Large deformations can be described, as in [10], with the so-called Cauchy-Green tensor

$$C = \begin{bmatrix} \lambda_1^2 & 0 & 0 \\ 0 & \lambda_2^2 & 0 \\ 0 & 0 & \lambda_3^2 \end{bmatrix}$$
 (3)

The principal strain described from a stretch ratio  $\lambda_1$ ,  $\lambda_2$  and  $\lambda_3$  results from the eigenvalues  $\lambda_1^2$ ,  $\lambda_2^2$  and  $\lambda_3^2$ . Using the invariants, the deformation state can be quantitatively characterized independently of the coordinate system. Thus, the first invariant

$$I_1 = Spur(\mathbf{C}) = \lambda_1^2 + \lambda_2^2 + \lambda_3^2$$
 (4)

the change in length of the space diagonal spanned by the eigenvalues. The second invariant

$$I_{2} = \lambda_{1}^{2} \lambda_{2}^{2} + \lambda_{2}^{2} \lambda_{3}^{2} + \lambda_{1}^{2} \lambda_{3}^{2}$$
 (5)

describes the change of the surface and the third invariant the volume change.

$$I_3 = \det(\mathbf{C}) = \lambda_1^2 \lambda_2^2 \lambda_3^2 \tag{6}$$

Material models or constitutive laws describe the mechanical behavior of a material. Material models link stresses with strains. Stress-strain curves from experiments are used to characterize the material behavior. Uniaxial, equiaxial, and biaxial tests can be distinguished for elastomers. *Fig. 2.* shows two examples of typical material behavior.

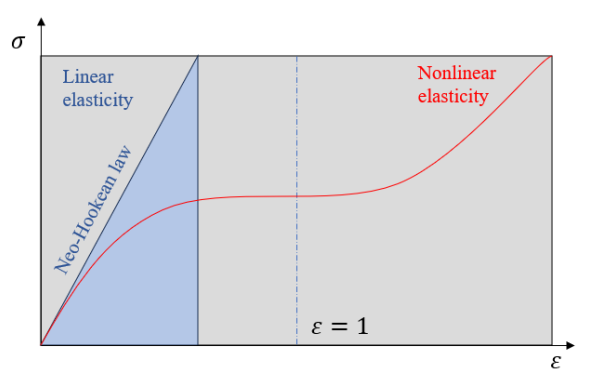


Fig. 2. Linear and nonlinear material behavior

One of the simplest constitutive laws is Hooke's law [9]. This results in the linear relationship between the triaxial stress state and the resulting strain state via the stiffness or elasticity tensor E:

$$\sigma = E \cdot \varepsilon \tag{7}$$

Hooke's law is only valid for small strains and is therefore only partially suitable for describing the material behavior of elastomer materials. The large elastic deformations of elastomers lead to geometric nonlinearities, which is why the relationship between stress  $\sigma$  and strain  $\varepsilon$  cannot be described using equation (7). The mechanical behavior of elastomer components is often described using hyperelastic material models. These are time-independent material models [11, 12,



13], and can be used to approximate nonlinear-elastic and incompressible material behavior in quasi-static considerations.

An alternative approach to describing the relationship between stress and strain is the concept of strain energy density. If one restricts oneself to the linear relationship according to equation (7), the volume-specific strain energy can be described by

$$\Pi_{i} = \mathbf{E} \int_{0}^{\varepsilon} \varepsilon d\varepsilon = \frac{1}{2} \mathbf{E} \varepsilon^{2}$$
 (8)

In the stress-strain diagram shown in *Fig. 2.*, the strain energy corresponds to the area between the Hooke's line and the abscissa. Detailed information on the derivation can be found in [10-13].

To describe the nonlinear material behavior of elastomers, we exploit the fact that, in principle, any mathematical function can be represented by a polynomial. Accordingly, the strain energy can be expressed as a polynomial in the invariants of the Cauchy-Green tensor as described by

$$\Pi_{i} = \sum_{i+j=1}^{n} C_{ij} \left( I_{1} - 3 \right)^{i} \left( I_{2} - 3 \right)^{j} \quad (9)$$

where  $C_{ij}$  is a material parameter and n is the degree of order of the polynomial. A frequently used hyperelastic material model is the Mooney-Rivlin model according to [14, 15], where the strain energy density is determined by a polynomial of degree n = 1 according to equation (9).

$$\Pi_{i} = C_{10} (I_{1} - 3) + C_{01} (I_{2} - 3)$$
 (10)

A special case of the Mooney-Rivlin model is the Neo-Hooke model, where  $C_{01} = 0$  and equation (10) is simplified to

$$\Pi_{i} = C_{10} \left( I_{1} - 3 \right) \tag{11}$$

Both the Mooney-Rivlin model from equation (10) and the Neo-Hooke model from equation (11) neglect the inflection

point in the stress-strain curve. The Yeoh model according to [16] is formulated non-linearly in the first invariant  $I_1$  and results in

$$\Pi_{i} = C_{10} (I_{1} - 3) + C_{20} (I_{1} - 3)^{2} + C_{30} (I_{1} - 3)^{3}$$

$$+ C_{30} (I_{1} - 3)^{3}$$
(12)

This allows the inflection point in the stress-strain curve to be described. The advantage of the Yeoh model and the Neo-Hooke model is that they only depend on the first invariant  $I_1$ . Therefore, considering one type of loading is sufficient.

The finite element method (FEM) is an approximate method for solving boundary value problems for partial differential equations. It is primarily used for field problems in heat conduction, fluid mechanics, electromagnetics and acoustics, but also primarily for structural mechanics problems. A detailed description is omitted below and reference is made to widely used standard works [17, 18, 19]. For further explanations on the application of FEM in the calculation of elastomer components, reference is made to [20, 21].

A general problem in the calculation of physical field problems is that an analytical solution exists for only a very few computational domains. The basic idea of FEM, as well as other approximation methods, is the spatial subdivision or discretization of an arbitrarily shaped domain into geometrically simple sub-fields, so-called finite elements. These finite elements are connected to each other via points also referred to as nodes. In this way, for example, a real, elastic continuum with an infinite number of degrees of freedom can be transformed into a discrete system with a finite number of degrees of freedom. The behavior of the field functions within the elements can be approximated by so-called form or shape functions.

For any elastic body, the total potential is generally calculated from the balance of internal  $\Pi_i$  and external potential  $\Pi_a$  as



$$\Pi = \Pi_{i} + \Pi_{a} = \frac{1}{2} \int_{\Omega} \tilde{\varepsilon}^{T} \tilde{\sigma} d\Omega - \int_{\Omega} u^{T} f_{\Omega} d\Omega - \int_{\partial\Omega} u^{T} t d\partial\Omega$$
(13)

The stress tensor from equation (1) and the strain tensor from equation (2) are converted into the vectorial notation  $\tilde{\sigma}$  and  $\tilde{\varepsilon}$  using, for example, Voigt's notation. The so-called stress or traction vector  $t = \sigma^T \cdot n$  contains the area-related forces and f the volume-related forces. According to the principle of virtual displacement, virtual work is

Here, the stiffness matrix **K** depends on the initially unknown displacement vector  $\hat{u}$ , which requires iterative solution methods.

### Mesh Approach for 3D FEA of a Radial Shaft Seal (RSS)

For the purposes of the current paper a 0.1° 3D segment of RSS is used which is transformed to finite element mesh consisting of different sizes of each element. *Fig. 3.* presents the mesh structure with 5 groups of mesh elements. In total, the FEM counts 290000 nodes and 270000 finite elements.

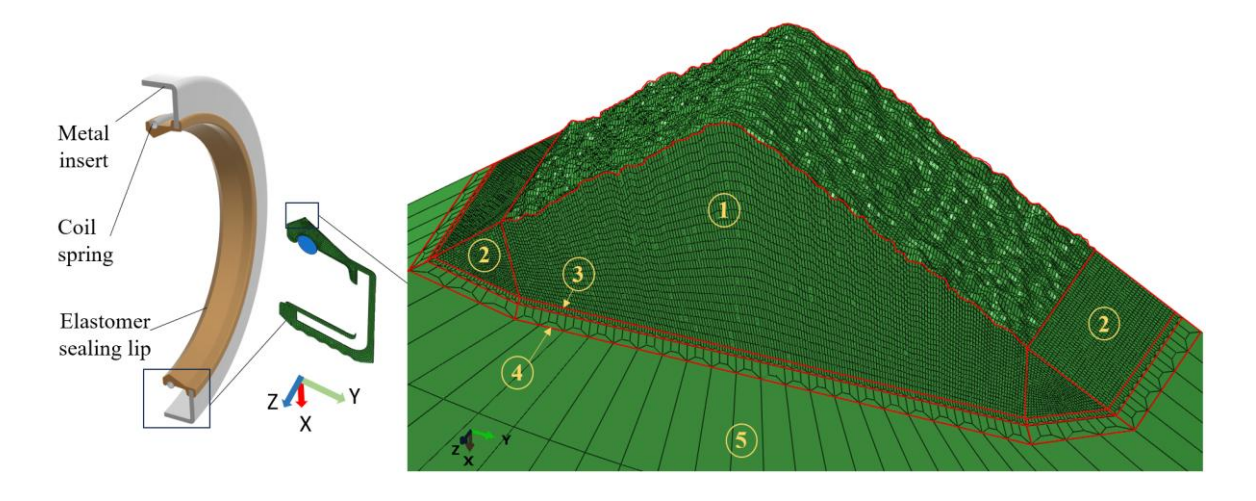


Fig. 3. 3D mesh structure of RSS sealing edge.

$$\delta\Pi = \delta\Pi_{i} + \delta\Pi_{a} = \int_{\Omega} \delta\tilde{\varepsilon}^{T} \tilde{\sigma} d\Omega$$
$$-\int_{\Omega} \delta u^{T} f_{\Omega} d\Omega - \int_{\partial\Omega} \delta u^{T} t d\partial\Omega = 0$$
 (14)

where  $\delta$  means an infinitesimal change of the potentials with an infinitesimal change of the displacements u.

The above explanations are intended to introduce the basic approach of FEM and are therefore limited to linear problems.

The final form of the equations used in FEA is

$$\Psi(\hat{\mathbf{u}}) = \mathbf{K}(\hat{\mathbf{u}})\hat{\mathbf{u}} - \hat{f} = 0 \tag{15}$$

The coarse bulk mesh is denoted as region 5 and includes the bigger part of the model far from the sealing edge with average dimension of elements 0.2 mm to 8 µm. Getting closer to the sealing edge there are two transition groups 4 - mesh transition 6 to 2 μm and 3 - mesh transition 2 to 0.7 µm. A transition element structure is shown on Fig. 4., created using isoparametric element approach - random physical elements coordinates to be transformed in natural coordinates and vice versa from one element to thirteen smaller elements created. Group 2 is interspace between sealing edge and mesh transition 3 with element size of 0.0005 mm. The last group 1 is scoping the target zone



which is the exact sealing edge which afterwords is in contact with the shaft. The roughness structure is based on Schallamach [22] who examined the contact of a compliant rubber specimen with a rigid glass counterpart. He concluded that the micro-asperities of the rough rubber surface orient perpendicularly to the direction of movement due to shear stresses, creating detachment waves. The waves in the current case are orientated along the shaft axis with  $Rz = 1.605 \mu m$ . The surface micro-asperities are generated so that when the segment of 0.1° is patterned around the shaft/seal axis, there is a perfect matching between the end side of one segment to the beginning side of the next segment, which is a good prerequisite for further EHL or CFD analysis.

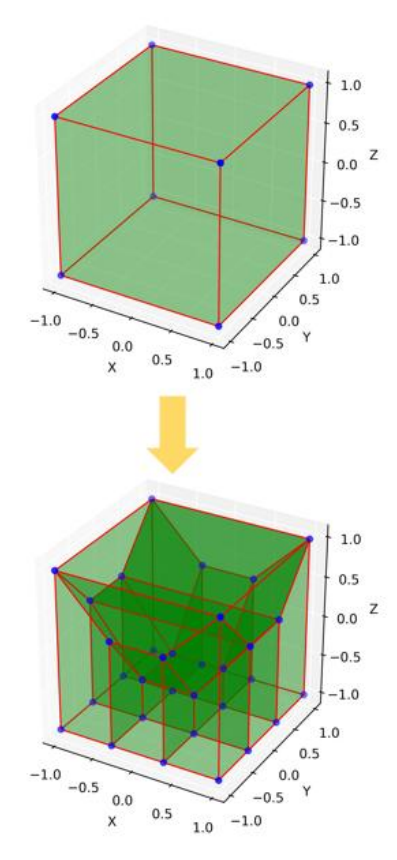


Fig. 4. 3D transition mesh element structure

#### **Problem Statement**

For the sake of the current study, a typical geometry of RSS type TRA 50 x 65 x 7, provided by Trelleborg Sealing Solutions, was

used. The part has a nominal inner diameter of d = 50 mm, and its elastomeric sealing part is made of nitrile butadiene rubber

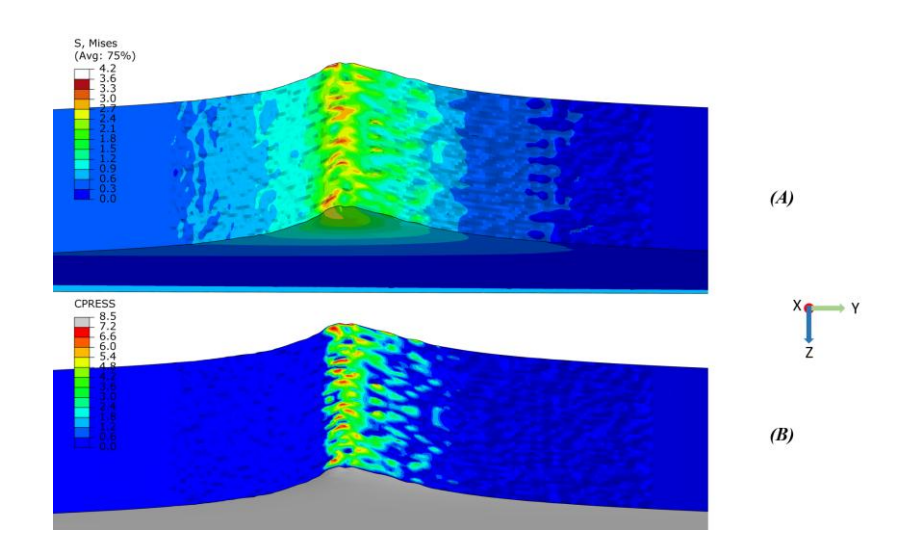


Fig. 5. (A) Stress Von-Mises (B) Contact pressure



(NBR) with a hardness of 75 Shore A. Furthermore, the parameter C<sub>10</sub>, assessed for the Neo-Hookean material model used for the FEA, was found to be 1.556 MPa value for ambient temperature. The shaft is considered a smooth rigid body, while the contact between the sealing edge and the shaft is defined as a node-to-surface pure penalty contact in the commercial software Abaqus. A constant coefficient of friction (COF) of 0.3 is defined for the seal-shaft contact. Cyclic symmetry boundary condition is applied on both sides of the seal cross section so that the distortion effect can be taken into account in the final outcome.

#### **Results**

The following results are obtained based on the previously presented FEA model. *Fig. 5.* and *Fig. 6.* show the von Mises stress and the contact pressure distribution between the sealing edge and the shaft. The contact stress denotes a contact bandwidth of 0.04 mm. The contact bandwidth – axial width of the contact – lies well within the expected range for a RSS in the new state after production. Both the highest von Mises stress and contact pressure are located at the oil side end of the contact bandwidth. The

average stress range is approximately 2.5 MPa. The contact pressure values are about 4.5 MPa.

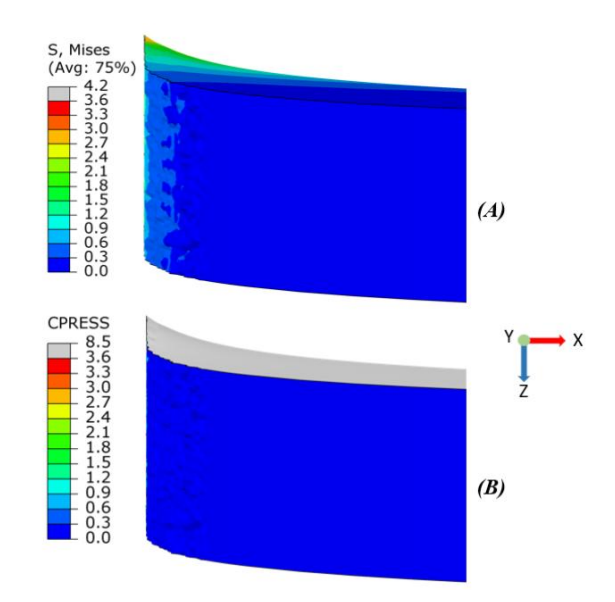


Fig. 6. (A) von Mises Stress
(B) Contact pressure.

The radial load for the simulated segment is 0.0029 N. This equals a total contact load for the complete seal of 10.44 N, valid for the defined operating temperature of 50 °C. Due to the deformations of the soft elastomer asperities onto the shaft, following the radial

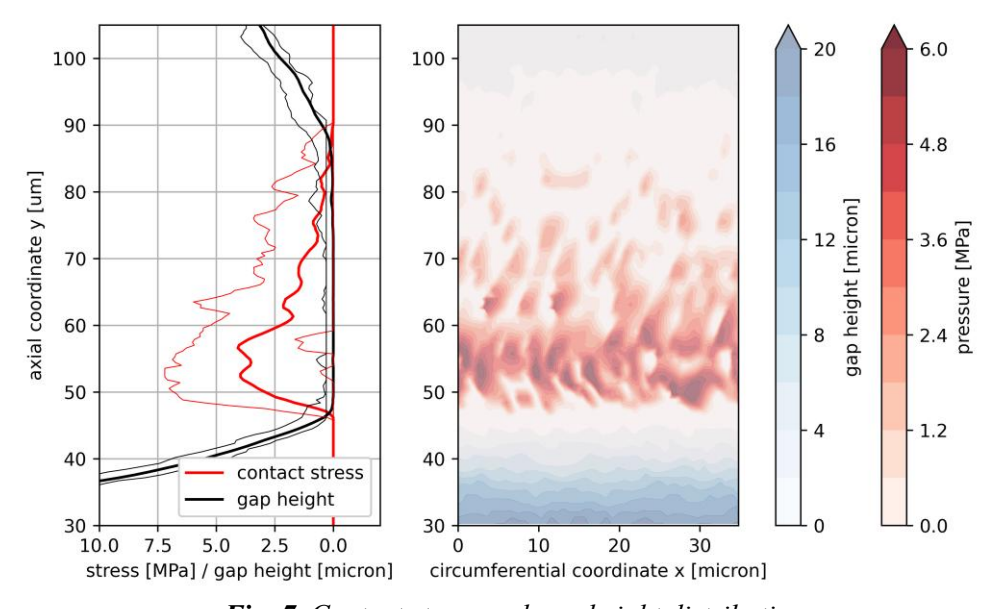


Fig. 7. Contact stress and gap height distribution



load from geometric overlap and the spring energizer, the contact area percolates, meaning that an uninterrupted contact area between the sealing edge and the shaft is formed in circumferential direction.

A contour plot diagram of the FEA results with cross-sectional view of mean, maximal and minimal contact stress and gap height distributions is shown in Fig. 7. The presented results offer an additional view on the distortion of the sealing edge as a result of the dynamic friction between the sealing edge and the shaft. Long tilted channels are formed on both sides of the contact stress apex. Due to the asymmetric pressure distribution, the tilted channels differ in length such that the air side channels are 3 times longer than the oil side ones. This observation correlates well with the previously introduced S value which amounts to 0.3 in the current case. This corresponds to 70% safety margin for the new state of the sealing edge after production. It should be noted that after break-in and with continuous wear during the lifetime of the seal, the S value is expected to increase.

#### **CONCLUSION**

This study presents a numerical method for performing structural analyses of radial shaft seals. There is a detailed description of the creation of a three-dimensional multiscale model for the purpose of simulating the microscopic interaction in the contact region between the sealing edge and the shaft surface. A new mesh generation technique is developed and applied. Material properties and boundary conditions used in the study are described. A numerical method is used to generate rough surfaces on the sealing edge. The results shed light on the micromechanical contact deformations in radial lip seals. Additionally, this article discusses the rotation-induced deformations of the shaft. As such, the tangential distortions of the sealing edge surface in the circumferential direction, which had been determined previously by

means of optical investigations, are corroborated. With this confirmation, it becomes possible to set up a relationship between the pressure distribution and the local tangential deformation of the sealing contact for ideally smooth as well as rough surfaces. The sealing edge distortion principle set forth by Kammüller is thus numerically verified. The obtained results set the basis for the analysis of hydrodynamic effects within the sealing gap. As such, the methodology presented forms the basis for an in-depth analysis of the lubrication and sealing behavior characteristics of radial lip seals.

#### REFERENCE

- [1] D. Frölich, B. Magyar, B. Sauer, A comprehensive model of wear, friction and contact temperature in radial shaft seals, Wear 311 (2014) 71.
- [2] J. Grün, S. Feldmeth, F. Bauer, Wear on radial lip seals: a numerical study of the influence on the sealing mechanism, Wear 476 (2021) 203674.
- [3] J. Grün, S. Feldmeth, F. Bauer, The sealing mechanism of radial lip seals: A numerical study of the tangential distortion of the sealing edge, Tribology and Materials 1 (2022) 1.
- [4] J. Grün, M. Gohs, F. Bauer, Multiscale Structural Mechanics of Rotary Shaft Seals: Numerical Studies and Visual Experiments, Lubricants 11 (2023) 234.
- [5] F. Guo, X. Jia, S. Suo, R.F. Salant, Y. Wang, A mixed lubrication model of a rotary lip seal using flow factors, Tribology International 57 (2012) 195.
- [6] M. Hajjam, D. Bonneau, Elastohydrodynamic analysis of lip seals with microundulations, Proceedings of the Institution of Mechanical Engineers Part J Journal of Engineering Tribology 218 (2004) 13.
- [7] X. Jia, F. Guo, L. Huang, L. Wang, Z. Gao, Y. Wang, Effects of the radial force on the static contact properties and sealing performance of a radial lip seal, Science China Technological Sciences 57 (2014) 1175.
- [8] W. Li, L.S. Stephens, Modeling Issues Associated With a Lip Seal Operating on a Textured Shaft, (2010) 61.



- [9] Ferdinand P. Beer, John T. Dewolf, David F. Mazurek, Mechanics of materials (7<sup>th</sup> edition) Hardcover, 896 Pages, Published 2014
- [10] I. Doghri: Mechanics of Deformable Solids: Linear, Nonlinear, Analytical, and Computational Aspects. Springer Berlin, Heidelberg, 2000.
- [11] U. Mohr-Matuschek: Auslegung von Kunststoff und Elastomerformteilen mittels Finite-Elemente-Simulationen. Bd. 68. Fortschritt-Berichte VDI Reihe 20, Rechnerunterstützte Verfahren 20. VDI-Verlag GmbH, 1992.
- [12] M.-C. Vöhringer: Prüfung und Beschreibung des mehrachsigen mechanischen Verhaltens von Elastomeren für die Finite-Elemente-Methode. 1. Aufl. IKV-Berichte aus der Kunststoffverarbeitung 199. Verlagsgruppe Mainz GmbH Aachen, 2009.
- [13] M. Stommel, M. Stojek und W. Korte: FEM zur Berechnung von Kunststoff und Elastomerbauteilen. Carl Hanser Verlag, 2011.
- [14] M. Mooney: "A Theory of Large Elastic Deformation". In: Journal of Applied Physics 11(9) (Sep. 1940), S. 582–592.

- [15] R. S. Rivlin: "Large elastic deformations of isotropic materials IV. Further developments of the general theory". In: Philosophical Transactions of the Royal Society of London. Series A, Mathematical and Physical Sciences 241(835) (5. Okt. 1948), S. 379–397.
- [16] O. H. Yeoh: "Some Forms of the Strain Energy Function for Rubber". In: Rubber Chemistry and Technology 66(5) (1. Nov. 1993), S. 754–771.
- [17] O.C.Zienkiewicz, R. L. Taylor, The Finite Element Method, Fifth edition, , ISBN-13: 978-0750650496.
- [18] Daryl L. Logan, A First Course in the Finite Element Method 6th Edition, ISBN-13: 978-1-305-63511-1.
- [19] M. G. Larson, F.Bengzon, Texts in Computational Science and Engineering, ISBN 978-3-642-33286-9.
- [20] M. A. Crisfield, Non-linear Finite Element Analysis of Solids and Structures.
- [21] J. Bonet, R. D. Wood, Nonlinear Solid Mechanics for Finite Element Analysis, ISBN-13: 978-1107115620.
- [22] A. Schallamach, Friction and abrasion of rubber, Wear, Volume 1, Issue 5, 1958, Pages 384-417.